Bioorg. Med. Chem. 46 (2021) 116345

Contents lists available at ScienceDirect

Bioorganic & Medicinal Chemistry

journal homepage: www.elsevier.com/locate/bmc

Biofunctional supramolecular hydrogels fabricated from a short self-assembling peptide modified with bioactive sequences for the 3D culture of breast cancer MCF-7 cells

Jyh Yea Chia, Takayuki Miki, Hisakazu Mihara, Hiroshi Tsutsumi *

School of Life Science and Technology, Tokyo Institute of Technology, Nagatsuta-cho 4259-B40, Midori-ku, Yokohama 226-8501, Japan

ARTICLE INFO

Keywords:
Self-assembling peptide
Bioactive sequences
Hydrogel
Cancer cell
3D culture

ABSTRACT

Self-assembling peptides are a type of molecule with promise as scaffold materials for cancer cell engineering. We have reported a short self-assembling peptide, $(FFiK)_2$, that had a symmetric structure connected via a urea bond. In this study, we functionalized $(FFiK)_2$ by conjugation with various bioactive sequences for the 3D culture of cancer cells. Four sequences, RGDS and PHSRN derived from fibronectin and AG73 and C16 derived from laminin, were selected as bioactive sequences to promote cell adhesion, proliferation or migration. $(FFiK)_2$, and its derivatives could co-assemble into supramolecular nanofibers displaying bioactive sequences and form hydrogels. MCF-7 cells were encapsulated in functionalized peptide hydrogels without significant cytotoxicity. Encapsulated MCF-7 cells proliferated under 3D culture conditions. MCF-7 cells proliferated with spheroid formation in hydrogels that displayed RGDS or PHSRN sequences, which will be able to be applied to drug screening targeting cancer stem cells. On the other hand, since MCF-7 cells migrated in a 3D hydrogel that displayed AG73, we could construct the metastatic model of breast cancer cells, which is helpful for the elucidation of breast cancer cells and drug screening against cancer cells under metastatic state. Therefore, functionalized $(FFiK)_2$ hydrogels with various bioactive sequences can be used to regulate cancer cell function for tumor engineering and drug screening.

1. Introduction

Tissue-engineered cancer models that mimic the *in vivo* tumor microenvironments have contributed not only to understanding the dynamic tumor development and progression but also to studies on cancer therapy.[1,2] Tissue engineering using functional scaffolds for cancer cell culture can contribute to the advancement of cancer biology research.[3] Most tumors in the human body exist within three-dimensional (3D) hydrogel milieus composed of complexed biomolecules, including extracellular matrix proteins and polysaccharides.[1] Conventional two-dimensional (2D) culture often poorly presents tumor conditions such as cell-cell interactions or signalling between cells residing within the outer proliferative regions and cells situated inside tumors.[4,5] On the other hand, 3D cancer cell culture systems have recently greatly promoted the understanding of the microenvironments that characterize tumor tissues, including cell-cell interactions and cell-ECM interactions. Various 3D biomimetic scaffolds from natural materials such as Matrigel,[6] alginate,[7] and collagen[8] and synthetic materials such as polyethene glycol (PEG)[2] have been used to construct tumor tissue models. Although these materials can create 3D scaffolds for cell growth, most of them lack mechanical or biochemical properties that promote cancer development. Molecular self-assembly is one of powerful approaches in the construction of functional materials for cancer tissue engineering. In particular, self-assembling peptides that can form hydrogels have attracted much attention for the construction of 3D cancer microenvironments, particularly EAK 16[9] and RADA-16.[10] Self-assembling peptides with either α-helix or *β*-sheet structure design can assemble into nanofibrous structures via noncovalent interactions and form hydrogels that can encapsulate cancer cells for 3D culture.[11,12]

Breast cancer is a leading cause of death. In previous studies, 3D breast cancer models have been developed with various biomimetic materials, such as PEG-fibrinogen,[2] PEG-heparin,[13,14] collagen,[15] chitosan[16] and Matrigel,[17] for the investigation of tumorigenic phenomena, for studies of tumor-associated cell population behaviour, and for anticancer drug testing. However, some of these materials, especially Matrigel, showed some structural weakness, which allowed only thin-

* Corresponding author.
E-mail address: htsutsum@bio.titech.ac.jp (H. Tsutsumi).

https://doi.org/10.1016/j.bmc.2021.116345
Received 1 June 2021; Received in revised form 27 July 2021; Accepted 30 July 2021
Available online 11 August 2021

layer and short-term analysis (<4 days).[18] Although a self-assembling peptide hydrogel was also used for the encapsulation and 3D culture of breast cancer cells, biological activity was not installed into the self-assembling peptide materials. [19]

Previously, we reported that a self-assembling peptide E1Y9 with an amphiphilic β-sheet structure could form the hydrogel as a cell culture scaffold.[20] E1Y9 peptide could be functionalized with bioactive sequences to enhance its cell adhesion activity and applied as a drug releasing carrier.[21,22] Recently, we reported a short self-assembling peptide, $(FFiK)_2$, that can fabricate a stable hydrogel in response to pH change (Fig. 1a).[23] $(FFiK)_2$ has a symmetric structure composed of two diphenylalanine (FF) units interconnected by a urea bond at the center and a lysine residue at each terminal via isopeptide bonds. Hydrophobic interactions between FF units and hydrogen-bonding networks of urea and amide bonds acted as the driving force for self-assembly, and electrostatic interactions at the zwitter ionic termini controlled the self-assembly in response to pH change. $(FFiK)_2$ assembles into supramolecular nanofibers at physiological pH and forms a stable and transparent hydrogel at final peptide concentrations as low as 0.5 wt%. The $(FFiK)_2$ hydrogel is a biocompatible material due to non-cytotoxic property. Since $(FFiK)_2$ is easy to synthesize on a large scale compared to other self-assembling peptides such as RADA16 and E1Y9 due to its simple and symmetric structure, we consider that $(FFiK)_2$ is a promising candidate material for the construction of larger tumor tissue models. However, $(FFiK)_2$ showed weak cell adhesion activity for cell culture. Therefore, functionalization of $(FFiK)_2$ is required for the 3D culture of cancer cells.

In this study, $(FFiK)_2$ was conjugated with various bioactive sequences derived from extracellular matrix (ECM) proteins to improve the cell adhesion and growth activities for the 3D culture of cancer cells. The RGDS and PHSRN sequences derived from fibronectin are known to promote cell adhesion, while the AG73 and C16 sequences derived from laminin are known to enhance cancer cell adhesion and proliferation. These bioactive sequences were conjugated with $(FFiK)_2$ to produce tailored artificial ECMs. The self-assembling properties of $(FFiK)_2$ derivatives were investigated including the hydrogelation property. The contribution of installed bioactive sequences to adhesion and proliferation of MCF-7, a breast cancer cell line, for functionalized hydrogels was evaluated. In addition, $(FFiK)_2$ hydrogels that displayed bioactive sequences were applied to the 3D culture of MCF-7 cells. The relationship between bioactive sequences and cell behaviour in hydrogels was investigated to determine the proper bioactive sequences for the control of spheroid formation and metastatic activity of MCF-7 cells. This work could contribute to tumor engineering for spheroid formation related to cancer cell stemness and metastatic model of breast cancer cells toward drug screening targeting breast cancer cells.

2. Materials and methods

2.1. General

All chemicals and solvents were of reagent or HPLC grade and were used without further purification. Amino acid derivatives were purchased from Watanabe Chemical Industries, Ltd (Japan). Other chemical reagents and solvents were purchased from Fujifilm Wako Pure Chemical (Japan) and Tokyo Chemical Industry (Japan). NMR measurements were conducted using an Agilent UNITY-INOVA-400. ESI MS measurements were conducted using an LCMS-2010 (Shimadzu).

2.2. Synthesis of $(FFiK)_2$ derivative

$(FFiK)_2$ was synthesized according to a previous report.[23] The synthesis scheme of $(FFiK)_2$ using the liquid phase synthesis method was shown in Fig. S1. A single Boc group was removed from fully protected $(FFiK)_2$ and the partially deprotected $(FFiK)_2$ was used for conjugation with various bioactive sequences. The detailed experimental procedures are described in the supplementary data (Fig. S2-S3).

2.3. Solid phase peptide synthesis and conjugation of $(FFiK)_2$ with bioactive sequences

All bioactive sequences were synthesized using a solid-phase method based on standard Fmoc chemistry.[24] The syntheses were carried out on TentaGel S RAM resin (HiPep Laboratories, Japan) to yield *C*-terminal amides. Fmoc-protected amino acid (3 eq. for amino group on resin) was activated by 3 eq. of HOBt·H_2O and 3 eq. of HBTU in 2 mL of NMP with 6 eq. of DIEA. In the syntheses of biotinylated peptides, Fmoc-Lys(Biotin)–OH was used. After elongation, the *N*-termini of all the bioactive sequences were bromoacetylated using preactivated bromoacetic acid (20 eq.) by 10 eq. of *N,N′*-diisopropylcarbodiimide at room temperature

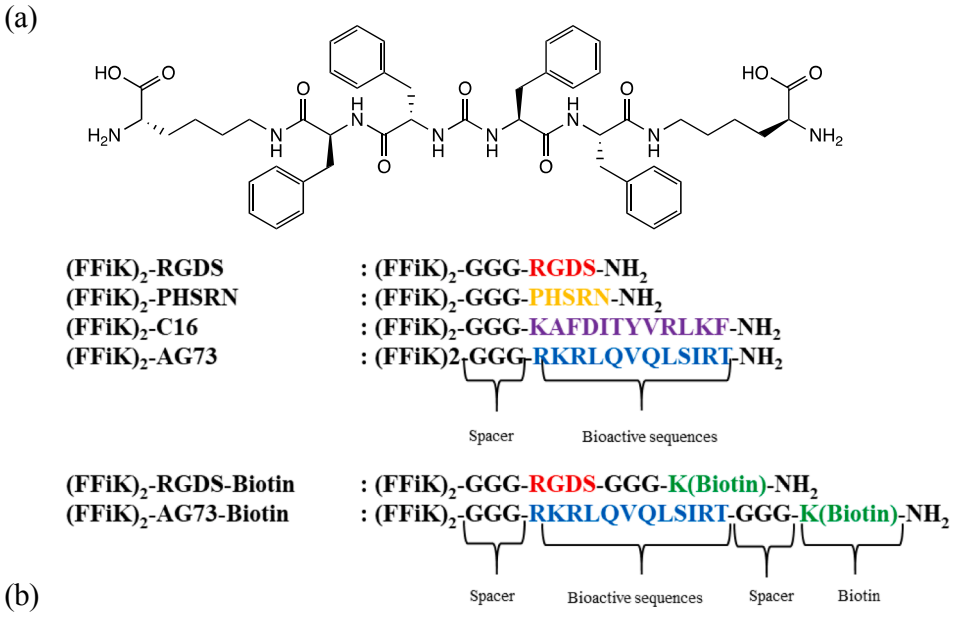

Fig. 1. Structure of $(FFiK)_2$ and peptide sequences of $(FFiK)_2$ derivatives (a) Chemical structure of $(FFiK)_2$. (b) Peptide sequences of $(FFiK)_2$ derivatives. The bioactive sequences derived from natural ECMs, RGDS, PHSRN, AG73 and C16, were conjugated with $(FFiK)_2$ peptide at *N*-terminus via a GGG linker, respectively.

for 30 min in 2 mL of NMP. Bromoactylated peptides were conjugated with $(FFiK)_2$ partially deprotected by the removal of a single Boc group (2 eq.) in 2 mL of NMP supplemented with potassium iodide (1 eq) and DIEA (1 eq.) at room temperature for 24 h. Cleavage of peptides and deprotection of side chains were performed with a mixture of trifluoroacetic acid (TFA) (95% v/v), triisopropylsilane (2.5% v/v) and water (2.5% v/v) for 1.5 h at room temperature. The crude peptides were then precipitated in cold diethyl ether, collected by centrifugation and dried under vacuum. All peptide purification was performed by reversed-phase HPLC on a COSMOSIL 5C18-ARII packed column (10 × 250 mm) with a linear gradient of acetonitrile containing 0.08% (v/v) TFA and ultrapure water containing 0.1% (v/v) TFA at a flow rate of 3 mL/min. The purified peptide was lyophilized to obtain peptides as powder. The products were identified by electrospray ionization mass spectrometry (ESI-MS). The ESI-MS results are shown in Table S1 (supplementary data).

2.4. Attenuated total reflection infrared (ATR-IR) spectroscopy

$(FFiK)_2$, $(FFiK)_2$-RGDS, $(FFiK)_2$-PHSRN, $(FFiK)_2$-AG73 and $(FFiK)_2$-C16 were dissolved in ultrapure water with the addition of 4 eq. of 1 M NaOH solution to prepare 1 mM solutions, respectively. Then, 2 eq. of HCl_{aq} was added to the peptide solutions to neutralize the peptide solution and incubated at room temperature for 48 h prior to ATR-IR measurement. A 10 μL of each peptide solution was mounted on the reflective surface of an FT-IR instrument (IRPrestige-21 with DuraSampl IR-II, Shimadzu) and air-dried to form a peptide film. ATR-IR spectra were obtained from 1300 cm^{-1} to 1800 cm^{-1} with the interferograms coadded 100 times and Fourier transformed at a resolution of 4 cm^{-1}.

2.5. Transmission electron microscopy (TEM)

$(FFiK)_2$, $(FFiK)_2$-RGDS, $(FFiK)_2$-PHSRN, $(FFiK)_2$-AG73 and $(FFiK)_2$-C16 were dissolved in ultrapure water with the addition of 4 eq. of 1 M NaOH solution to prepare 1 mM peptide solutions, respectively. The peptide solutions were further diluted to 100 μM with ultrapure water containing 2 eq. of HCl to neutralize the peptide solution. The diluted solutions were incubated at room temperature for 48 h prior to TEM grid coating. A collodion-coated copper EM grid was glow discharged for 40 *sec* at 3 mA using an IB2 ion coater. A 10 μL of peptide solution was mounted on the collodion-coated copper EM grid for 30 *sec* to adsorb the peptide nanofibers. The excess solution was removed by capillary action with filter paper, and the grid was washed by adding a drop of ultrapure water (10 μL). After removal of the ultrapure water, the grids were stained twice with 10 μL of NanoW staining solution (2% solution in water at pH 6.8) (Nanoprobes) for 1 min each time. The stained grids were blotted with filter papers and allowed to dry at room temperature overnight. TEM images were taken with a JEM 1400Plus (JEOL) that was operated at 80 kV.

Mixed solutions of $(FFiK)_2$ and biotin-modified $(FFiK)_2$ derivatives (10 wt%) were prepared as 100 μM solutions in ultrapure water by the same procedure described above. After 48 h of incubation, 10 μL of peptide solution was mounted on the collodion-coated copper EM grid for 30 *sec* to adsorb the peptide nanofibers. The excess solution was removed by capillary action with filter paper, and the grid was washed by adding a drop of ultrapure water (10 μL). After removal of the ultrapure water, 10 μL of the streptavidin-gold nanoparticle (10 nm) conjugates (streptavidin-GNP) (Cytodiagnostics) was mounted on the collodion-coated copper EM grid for 1 min. After removal of excess streptavidin-GNP by capillary action with filter paper, the grid was washed by adding 10 μL of ultrapure water. Then, the sample was stained with NanoW by the same procedurer described above, and TEM images were taken.

2.6. Hydrogelation analysis

Mixtures of $(FFiK)_2$ and $(FFiK)_2$-bioactive sequences (molar ratio = 4/1) were dissolved in ultrapure water containing 4 eq. of NaOH to prepare a total 1.0 wt% peptide solution. A 100 μL aliquot of peptide solution was mixed with 100 μL of RPMI-1640 without phenol red to prepare a 0.5 wt% solution. After incubation at room temperature for 30 min, hydrogelation was confirmed by inverting the glass vial.

2.7. Cell culture

MCF-7 cells were obtained from the RIKEN BRC. The cell line was tested and authenticated by the RIKEN BRC. MCF-7 cells were maintained in RPMI-1640 medium supplemented with 10% fetal bovine serum (FBS), 100 U/mL penicillin and 100 μg/mL streptomycin. The cells were cultured on Petri dishes and grown until reaching 80% confluence at 37 °C under 5% CO_2.

2.8. Cell adhesion on hydrogels

$(FFiK)_2$/$(FFiK)_2$-bioactive sequences (molar ratio = 4/1) were dissolved in sterile water with 4 eq. of NaOH to prepare 1.0 wt% peptide solutions. Aliquots of the peptide solutions (150 μL) were placed in 24-well nontreated plate (Falcon) and mixed with 150 μL of culture medium (RPMI-1640 supplemented with 1% penicillin- streptomycin) to prepare 0.5 wt% hydrogels. After incubation at 37 °C under 5% CO_2 for 30 min, 1.0×10^5 MCF-7 cells in serum-free RPMI 1640 (300 μL) were added on top of the hydrogels. The cells were incubated at 37 °C under 5% CO_2, and the number of adhered polygonal-shaped cells and non-adhered round-shaped cells were counted under a microscope (Ti-U-PH-1, Nikon) after 6 h of incubation. The average percentages of adhered cells/total cells were calculated using 3 different views from the same well. Statistical significance was accepted at $p < 0.05$.

2.9. Cell proliferation on/in hydrogels

sfGFP-MCF-7 cells (5.0×10^3) were cultured on hydrogels prepared in a 96-well tissue culture plate for 7 days with medium changes every two days. Cell proliferation was evaluated using a Cell Counting Kit-8 (CCK-8) colorimetric assay (Dojindo) at 1, 3, 5 and 7 days according to the manufacturer's instructions. The absorbance at 450 nm was measured on a microplate reader (ARVO MX, PerkinElmer) using a 450 nm filter.

The sfGFP-MCF-7 cells (5.0×10^3) encapsulated within hydrogels were cultured in a 96-well tissue culture plate for 10 days with medium changes every two days. Cell proliferation was evaluated in the same manner described above.

In 2D and 3D cell culture experiments, three wells were used for each condition. Error bars represent standard deviations (SD) of the means of three independent experimental values. Statistical significance was accepted at $p < 0.05$.

2.10. 3D cell culture in hydrogels

The MCF-7 cell line stably expressing sfGFP (sfGFP-MCF-7) was established and used for the 3D cell culture experiment. The detailed procedure for the establishment of sfGFP-MCF-7 is described in the supplementary data. $(FFiK)_2$/$(FFiK)_2$-bioactive sequences (molar ratio = 4/1) were dissolved in sterile water with 4 eq. of NaOH to prepare 1.0 wt% peptide solutions and incubated at 4 °C for 24 h prior to hydrogel preparation. Aliquots of the peptide solutions (50 μL) were placed in 96-well glass bottom plates (Iwaki) and mixed with RPMI-1640 supplemented with 1% penicillin-streptomycin containing 5.0×10^3 sf-GFP-MCF-7 cells to prepare 0.5 wt% of hydrogels. The hydrogels were incubated at 37 °C under 5% CO_2 for 30 min. After hydrogelation, 100 μL of RPMI-1640 supplemented with 10% FBS and 1% penicillin-

streptomycin was added to the hydrogels. The cells were incubated at 37 °C under 5% CO_2 with medium changes every two days and observed under a laser scanning confocal microscope (LSM780, Carl Zeiss) on days 1, 3, 5, 7 and 10.

2.11. Immunofluorescence staining

MCF-7 cells (1×10^5) were cultured in hydrogels for 10 days. The MCF-7 cell clumps were collected from the hydrogel by gentle resuspension using a pipette and centrifuged at 1100*g*. The supernatant was removed, and the cells were fixed with 4% paraformaldehyde for 1 h in a microcentrifuge tube and further permeabilized with 0.5% Triton-X 100 in PBS for 10 min at room temperature. Cell clumps were washed with PBS for three times by gentle resuspension and centrifugation. Cell clumps were blocked with 0.5% BSA for 1 h at room temperature in microcentrifuge tubes and centrifuged at 1100*g* to remove the blocking reagent. The primary antibody (rabbit anti-E-cadherin EP700Y intercellular junction marker, ab40772, 1:500 dilution, Abcam) was incubated for 1 h at room temperature with shaking, and followed by the secondary antibody [goat anti-rabbit IgG H&L (Alexa Fluor ® 488), ab205718, 1:200 dilution, Abcam] for 1 h at room temperature with shaking. The cells were washed three times for 5 min each in 0.1% Tween 20 in PBS, then incubated with Alexa-633-phalloidin (Phalloidin-iFluor 633, ab176758, Abcam) and DAPI for 30 min and washed three times with PBS. Finally, the cells were transferred to 96-well glass bottom plates (Iwaki) and observed under a confocal microscope.

2.12. Western blotting analysis of E-cadherin

After cell culture in peptide hydrogels, the cells were lysed with 100 μL of RIPA lysis buffer [50 mM Tris-HCl (pH 7.6), 150 mM NaCl, 1% (w/v) Nonidet P40 substitute, 0.5% (w/v) sodium deoxycholate, 0.1% (w/v) SDS)] supplemented with a cocktail of protease inhibitor (Sigma-Aldrich) for 1 h with rotation at 4 °C. Cell lysates were centrifuged at 17,000*g* for 15 min at 4 °C. The supernatant was harvested to obtain the whole cell proteins, and the protein concentration was determined by a BCA protein concentration kit (Takara Bio). 30 μg of protein from each sample was mixed with Laemmli sample loading buffer for SDS-PAGE. After transfer to PVDF membranes (Immobilon®-P, Merck) using a semidry transfer cell device (Bio-Rad), the blots were incubated with blocking buffer (5% skim milk) for 1 h at room temperature. Blots were incubated with primary antibodies against E-cadherin (rabbit anti-E-cadherin EP700Y intercellular junction marker, ab40772, 1:20,000 dilution, Abcam) and GAPDH [(D16H11)XP® rabbit mAB, 1:5000, Cell Signalling Technology] overnight at 4 °C and further incubated with secondary antibody (anti-rabbit IgG, HRP linked antibody #7074, Cell Signalling Technology) for 1 h at room temperature. The blot was visualized by SuperSignal West Femto Maximum Sensitivity Substrate (Thermo Scientific) according to the manufacturer's instruction and observed by LuminoGraph I (Atto). Quantitative image analysis was performed with ImageJ.

3. Results and discussion

3.1. Design of $(FFiK)_2$ functionalized with bioactive sequences

The $(FFiK)_2$ peptide (Fig. 1a) was synthesized according to our previous report.[23] To enhance the biological properties of $(FFiK)_2$, we conjugated $(FFiK)_2$ with various bioactive sequences derived from natural ECM proteins. The sequence RGDS derived from fibronectin was chosen to enhance the cell adhesion of a $(FFiK)_2$ hydrogel, because RGDS has been reported to promote cell adhesion when it is displayed on the surface of the materials.[25,26] The sequence PHSRN, which enhances cell adhesion synergistically with RGDS[26,27] was chosen as another bioactive sequence derived from fibronectin. Both AG73 (RKRLQVQLSIRT) and C16 (KAFDITYVRLKF) were chosen from laminin proteins, because these two sequences were reported to promote cancer cell adhesion and enhance tumor growth and tumor cell metastasis.[28,29] $(FFiK)_2$ was conjugated with RGDS, PHSRN, AG73 or C16 at the primary amine of $(FFiK)_2$ via a GGG linker to produce $(FFiK)_2$-RGDS, $(FFiK)_2$-PHSRN, $(FFiK)_2$-AG73 and $(FFiK)_2$-C16, respectively (Fig. 1b, Fig. S4). The partially deprotected $(FFiK)_2$ precursor (Fig. S2) was successfully allowed to react with bioactive sequences that had a bromoacetyl group at the *N*-terminus on the solid support. After cleavage from the solid support and HPLC purification, $(FFiK)_2$ derivatives were obtained in approximately 39–68% yields on solid phase peptide synthesis (Table S1).

3.2. Structure analysis of $(FFiK)_2$ derivatives in self-assembly

To demonstrate the potential of all $(FFiK)_2$ derivatives in β-sheet formation, attenuated total reflection infrared (ATR-IR) spectra were measured. The $(FFiK)_2$ and $(FFiK)_2$ derivatives showed predominant peaks around 1620–1640 cm^{-1} that were assigned to a β-sheet structure[30] (Fig. 2). This result suggests that all $(FFiK)_2$ derivatives could assemble into a β-sheet structure. The shoulder peaks around 1670 cm^{-1} of $(FFiK)_2$-PHSRN and $(FFiK)_2$-AG73 might come from a random structure of bioactive sequences conjugated with $(FFiK)_2$.

Self-assembled nanostructures of $(FFiK)_2$ and $(FFiK)_2$ derivatives were evaluated by TEM observation. $(FFiK)_2$ (Fig. 3a) and $(FFiK)_2$-RGDS (Fig. 3b) formed nanofibers with widths of approximately 8 nm and 10 nm, respectively. This result suggests that the RGDS sequence does not alter the self-assembling property of $(FFiK)_2$. On the other hand, $(FFiK)_2$-PHSRN, $(FFiK)_2$-AG73 and $(FFiK)_2$-C16 did not form uniform nanofiber structures like $(FFiK)_2$ (Fig. S5). $(FFiK)_2$-PHSRN, $(FFiK)_2$-AG73 and $(FFiK)_2$-C16 have + 1, +4 and +2 net charges, respectively; on the other hand, $(FFiK)_2$ and $(FFiK)_2$-RGDS are neutral. Electrostatic repulsion due to the conjugated sequences might affect the self-assembly of $(FFiK)_2$ derivatives.

Next, we tried to display bioactive sequences on assembled nanofibers by the co-assembly of $(FFiK)_2$ derivatives with a parent $(FFiK)_2$. For this purpose, 10 mol% of $(FFiK)_2$-RGDS, $(FFiK)_2$-AG73, or their

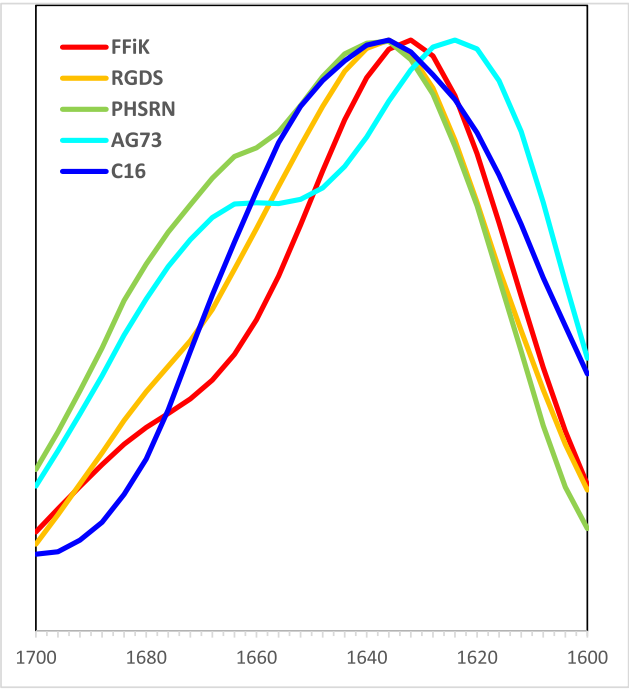

Fig. 2. ATR-IR spectra of $(FFiK)_2$, $(FFiK)_2$-RGDS, $(FFiK)_2$-PHSRN and $(FFiK)_2$-AG73 after incubation over 48 h. All spectra were measured from air-dried peptide films.

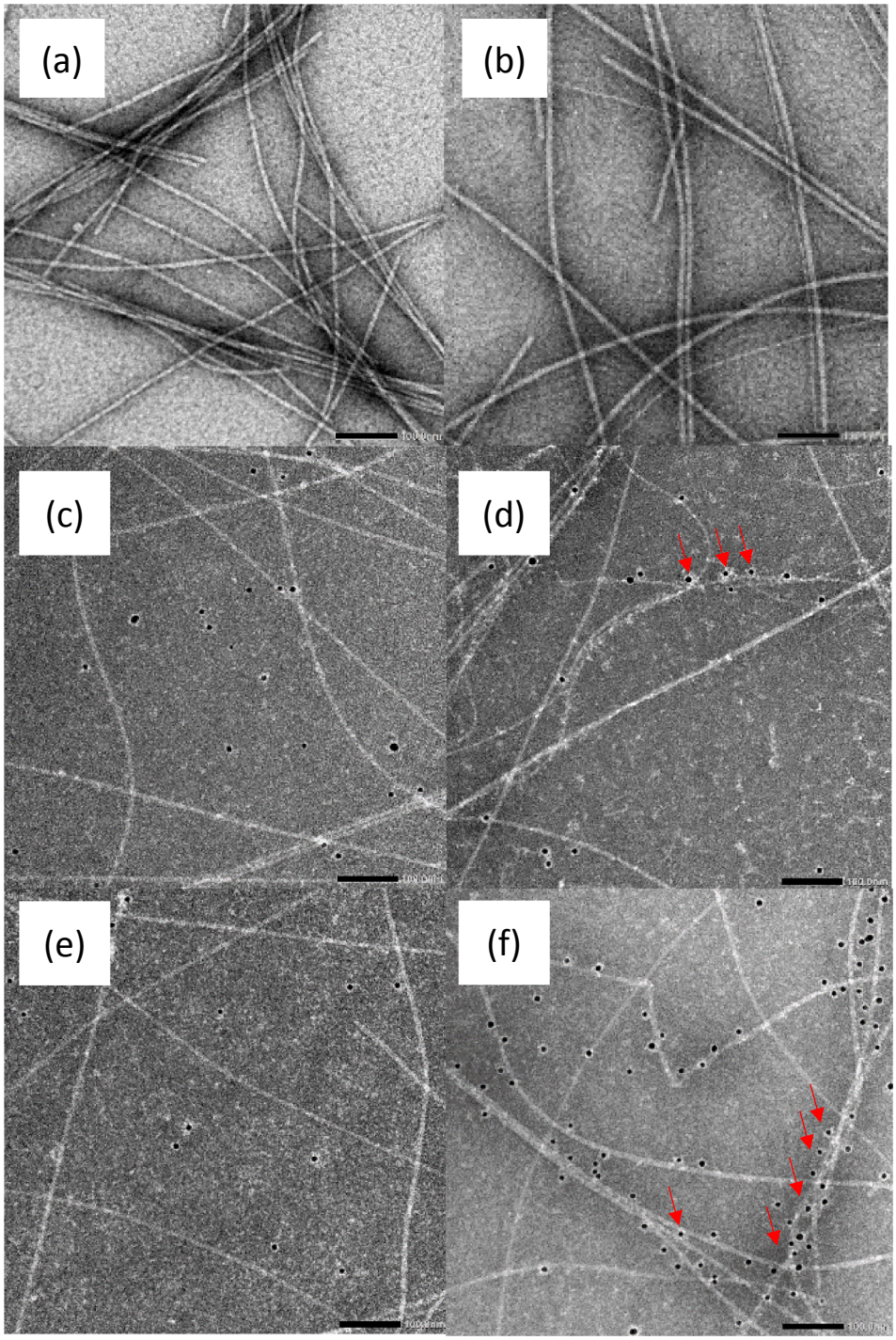

Fig. 3. TEM images of (a) $(FFiK)_2$, (b) $(FFiK)_2$-RGDS, (c) 10% $(FFiK)_2$-RGDS, (d) 10% $(FFiK)_2$-RGDS-Biotin, (e) 10% $(FFiK)_2$-AG73 and (f) 10% $(FFiK)_2$-AG73-Biotin in the presence of 10 nm streptavidin-conjugated gold nanoparticles. All samples were prepared in 100 μM and negatively stained using NanoW. Scale bar is 100 nm. Red arrow showed the position of 10 nm streptavidin-conjugated gold nanoparticles attached on the biotinylated peptide nanofibers.

biotinylated derivatives was mixed with $(FFiK)_2$. Both $(FFiK)_2$/$(FFiK)_2$-RGDS (10 nm width) and $(FFiK)_2$/$(FFiK)_2$-AG73 (13 nm width) showed long nanofibers with uniform width (Fig. 3c, e). This result indicates that the presence of $(FFiK)_2$-derivatives does not disturb the self-assembly of $(FFiK)_2$ peptides. To confirm whether bioactive sequences are displayed on nanofibers, co-assembled nanofibers of $(FFiK)_2$/$(FFiK)_2$-RGDS-Biotin and $(FFiK)_2$/$(FFiK)_2$-AG73-Biotin were labelled by streptavidin-gold nanoparticles (GNPs). Fig. 3d and f clearly show that GNPs were observed along with co-assembled nanofibers of $(FFiK)_2$/$(FFiK)_2$-RGDS-Biotin and $(FFiK)_2$/$(FFiK)_2$-AG73-Biotin, respectively. There were no GNPs on co-assembled nanofibers of $(FFiK)_2$/$(FFiK)_2$-RGDS (Fig.3c) and $(FFiK)_2$/$(FFiK)_2$-AG73 (Fig. 3e). These results suggest that $(FFiK)_2$ derivatives can co-assemble into nanofibers with the parent $(FFiK)_2$ and that bioactive sequences are displayed on the assembled nanofibers. Since not only the short sequence RGDS but also the long sequence AG73 was successfully displayed on nanofibers, various bioactive sequences can be used by the co-assembly method. Since highly cationic AG73 sequence of 12 residues could be displayed on self-assembled nanofibers, we considerd that the shorter PHSRN and less cationic C16 with the same amino acid length can be displayed on self-assembled

nanofibers in the same co-assembly manner.

3.3. Hydrogelation test

Hydrogelation tests of $(FFiK)_2$ and $(FFiK)_2$ derivatives were carried out to evaluate the macroscopic structure of the $(FFiK)_2$ and $(FFiK)_2$ derivatives. $(FFiK)_2$ derivatives and the parent $(FFiK)_2$ were mixed at a molar ratio of 1:4 to prepare a 0.5 wt% solution in cell culture medium. All peptide mixtures formed self-supporting hydrogels within 30 min of incubation at room temperature (Fig. 4). This result suggests that $(FFiK)_2$-conjugates with bioactive sequences of different lengths (4 to 12 residues) can form stable hydrogels by co-assembly with the parent $(FFiK)_2$. $(FFiK)_2$, $(FFiK)_2$-RGDS and $(FFiK)_2$-PHSRN gave transparent hydrogels, while $(FFiK)_2$-AG73 and $(FFiK)_2$-C16 formed slightly opaque hydrogels. This result indicates that the short sequences of $(FFiK)_2$-RGDS and $(FFiK)_2$-PHSRN disperse homogenously in hydrogels. On the other hand, the long sequences of $(FFiK)_2$-AG73 and $(FFiK)_2$-C16 might undergo partial aggregation in hydrogels due to their amphiphilic structures. However, these results show that $(FFiK)_2$ and $(FFiK)_2$ derivatives can co-assemble into networked nanofibers in the presence of high water content and form stable hydrogels. The parent framework of $(FFiK)_2$ has stable self-assembling ability enough to display long bioactive sequences of more than 10 residues even though $(FFiK)_2$ is a short peptide of 6 residues.

3.4. Cell adhesion on 2D hydrogels

Cell adhesion assays were performed to investigate the effect of bioactive sequences. The peptide hydrogels (0.5 wt%, molar ratio of $(FFiK)_2/(FFiK)_2$ derivatives = 4/1) were prepared in a 24-well microplate, and MCF-7 cells were cultured on the hydrogels for 6 h. The adherent percentages of MCF-7 cells were evaluated under a microscope (Fig. 5, Fig. S6). The hydrogels of $(FFiK)_2$, $(FFiK)_2/(FFiK)_2$-RGDS and $(FFiK)_2/(FFiK)_2$-PHSRN showed smooth surfaces, and MCF-7 cells adhered to the surface (Fig. S6a-c). On the other hand, the hydrogels of $(FFiK)_2/(FFiK)_2$-AG73 and $(FFiK)_2/(FFiK)_2$-C16 showed rough surfaces (Fig. S6d-e), probably due to partial aggregation of the bioactive sequences. The $(FFiK)_2$-AG73 hydrogel exhibited the highest cell adhesion activity (59%) among all hydrogels. The hydrogels functionalized with RGDS and C16 showed similar cell adhesion ability (38% and 44%, respectively). The $(FFiK)_2$-PHSRN hydrogel showed lower cell adhesion ability (26%) than the $(FFiK)_2$-RGDS hydrogel. In contrast, the $(FFiK)_2$ hydrogel showed only 10% cell adhesion activity. These results suggest that the bioactive sequences successfully improved the cell adhesion activity of the $(FFiK)_2$ hydrogel.

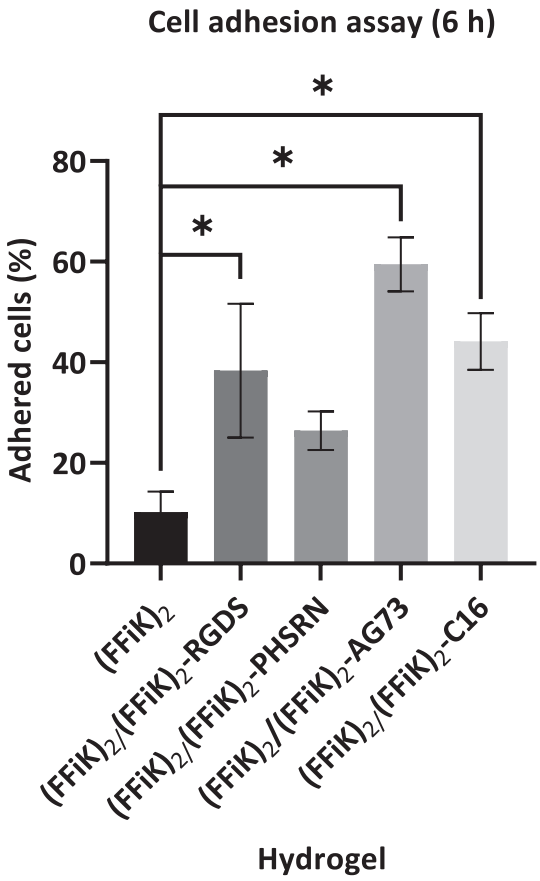

Fig. 5. Cell adhesion on $(FFiK)_2/(FFiK)_2$-derivative mixed hydrogels. The number of adhered cells on the hydrogel were counted and divided by the total number of cells and the average percentages were calculated using 3 different views. Error bar represent standard deviations (SD) of the means of three independent experimental value. Statistical significance was accepted at *p < 0.05.

Many of integrins expressed on the surfaces of cancer cells can recognize the tripeptide motif of RGD contained in the ECM proteins, and the interaction between integrins and the RGD motif promotes the adhesion and progression of cancer cells. [31] Therefore, installation of the RGDS sequence into $(FFiK)_2$ could improve the adhesion of MCF-7 cells. At first, the PHSRN motif was identified as a synergystic sequence that enhanced cell adhesion together with RGD sequence.[32] The PHSRN

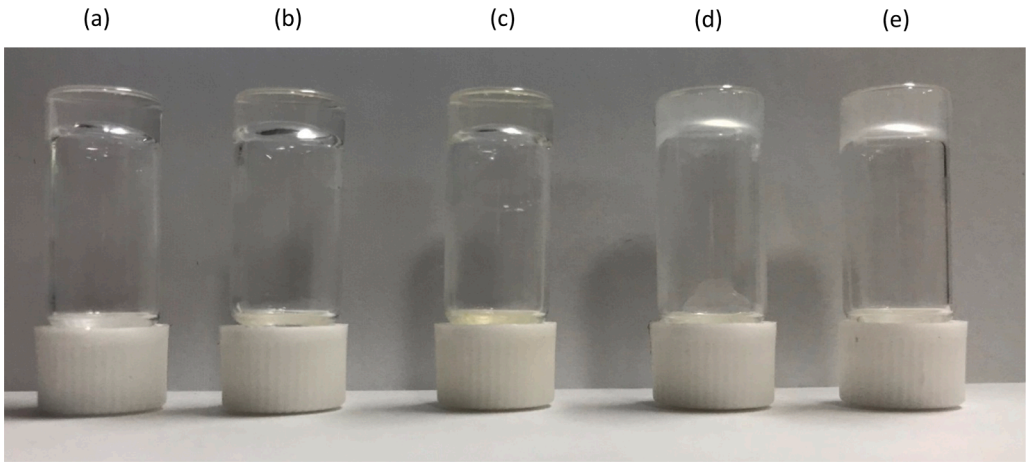

Fig. 4. Photographs of self-supporting hydrogels of $(FFiK)_2$ and $(FFiK)_2$ derivatives. (a) $(FFiK)_2$ (b) 20% $(FFiK)_2$-RGDS (c) 20% $(FFiK)_2$-PHSRN (d) 20% $(FFiK)_2$-AG73 (e) 20% $(FFiK)_2$-C16. The total concentration of peptides was 0.5 wt%.

peptide could promote cell adhesion, but its activity was weaker than the RGD peptide. Thereafter, the PHSRN sequence was reported to mediate cell adhesion through a common mechanism as the RGD motif but binds competitively to the integrin receptors with lower affinity rather than RGD.[33] These reports support that $(FFiK)_2$-PHSRN hydrogel exhibited higher cell adhesion than the $(FFiK)_2$ hydrogel but lower cell adhesion than $(FFiK)_2$-RGDS hydrogel. On the other hand, several types of breast cancer cells, including MCF-7 cells, strongly adhered to microplates coated with the AG73 peptide.[34] This report supports the highly improved adhesion activity of the $(FFiK)_2$-AG73 hydrogel. It was reported that C16 could bind to β1 integrin and promote the adhesion and migration of breast cancer cells through the regulation of GPNMB expression[35]; therefore, the $(FFiK)_2$-C16 hydrogel showed enhanced cell adhesion.

3.5. Cell proliferation on hydrogels (2D) and in hydrogels (3D)

Before the cell proliferation assay, the MCF-7 cell line stably expressing superfolder GFP (sfGFP-MCF-7) was established (Supporting data). In the cell proliferation assay, sfGFP-MCF-7 cell proliferation on hydrogels was monitored for up to 7 days by a WST assay using a CCK-8 kit (Fig. 6a). Fig. 6 shows the absorbance at 450 nm, which is related to the number of live cells. After 1 day of cultivation, the $(FFiK)_2$-AG73 hydrogel exhibited the highest cell numbers among all the tested conditions. In addition, the $(FFiK)_2$-AG73 hydrogel maintained the highest cell numbers over 7 days of cultivation. These results suggest that the AG73 sequence is the most effective in not only cell adhesion but also cell proliferation. The $(FFiK)_2$-C16 hydrogel exhibited the second highest cell proliferation activity among the hydrogels. This result reflects the cell adhesion activity, as shown in Fig. 6. In contrast to cell adhesion, the $(FFiK)_2$-RGDS and $(FFiK)_2$-PHSRN hydrogels did not markedly promote cell proliferation compared to the $(FFiK)_2$ hydrogel.

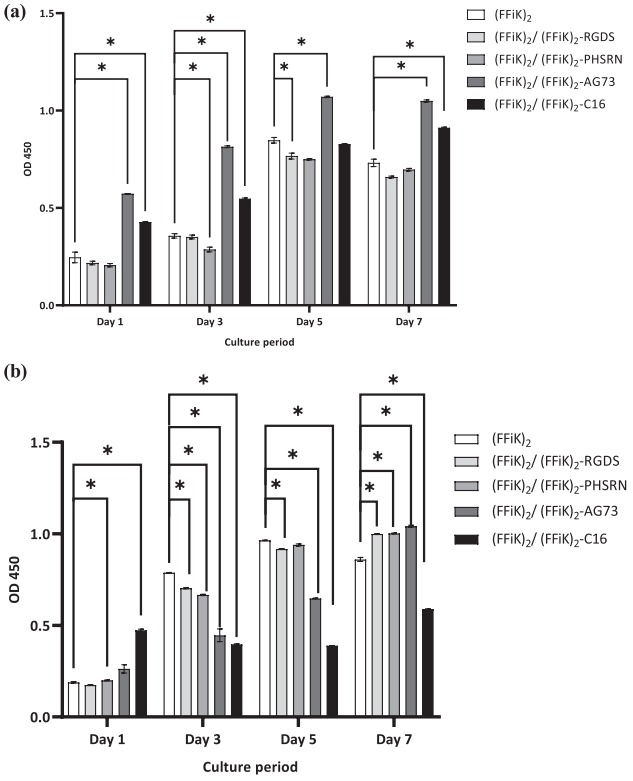

Fig. 6. Proliferation of sfGFP-MCF-7 cells over 7 days culture. Viable cells of 1, 3, 5 and 7 days cultured (a) on 2D hydrogel and (b) in 3D hydrogel. Error bar represent standard deviations (SD) of the means of three independent experimental value. Statistical significance was accepted at $*p < 0.05$.

This result implies that the improvement of the cell adhesion alone may be insufficient for the cell proliferation.

The proliferation of sfGFP-MCF-7 cells was also evaluated in 3D hydrogels (Fig. 6b). After 1 day of cultivation, the $(FFiK)_2$-C16 hydrogel exhibited the highest cell number among the hydrogels. However, significant cell proliferation was not observed in the $(FFiK)_2$-C16 hydrogel over 7 days of cultivation. The C16 peptide was reported to stimulate proteolytic activity, which eventually leads to cell apoptosis.[36,37] The combination of the increased number of dead cells observed with prolongation of the culture period and the proteolytic activity stimulated by the C16 peptide contributed to the low proliferation rate detected in sfGFP-MCF-7 cells (Fig. S8q-t). On the other hand, MCF-7 cells continuously proliferated in other hydrogels, and the $(FFiK)_2$-RGDS, $(FFiK)_2$-PHSRN and $(FFiK)_2$-AG73 hydrogels exhibited higher cell proliferation than the $(FFiK)_2$ hydrogel at day 7. This result indicates that RGDS, PHSRN and AG73 effectively promote cell proliferation in 3D hydrogels. Interestingly, the cell proliferation rates in these three hydrogels were different. In the 3D $(FFiK)_2$-AG73 hydrogel, the cell proliferation rate was slower than in the $(FFiK)_2$-RGDS and $(FFiK)_2$-PHSRN hydrogels, although the cell proliferation on the 2D $(FFiK)_2$-AG73 hydrogel was faster than that of the $(FFiK)_2$-RGDS and $(FFiK)_2$-PHSRN hydrogels (Fig. 6a). This difference might come from the 3D environment inside the hydrogels.

3.6. Cell imaging in 3D hydrogels

The sfGFP-MCF-7 cells were encapsulated within 0.5 wt% hydrogels of $(FFiK)_2$/$(FFiK)_2$ derivatives (molar ratio = 4/1) under well-dispersed conditions (Fig. S7). Encapsulated cells were cultured in hydrogels for 7 days (Fig. 7 and Fig. S8). Dead cells were stained by propidium iodide (PI). In the $(FFiK)_2$ hydrogel, MCF-7 cells proliferated with the spheroid formation (Fig. 7a). The size of spheroids was around 87 μm (Fig. 7f). A few cells were stained with PI over 7 days of cultivation. These results show that the $(FFiK)_2$ hydrogel enables the 3D culture of MCF-7 cells without significant cytotoxicity. Since the $(FFiK)_2$ hydrogel does not have positive adhesion activity for MCF-7 cells as demonstrated in the cell adhesion experiment, strong cell-cell interactions might cause the spheroid formation. In the case of the $(FFiK)_2$-RGDS hydrogel, MCF-7 cells formed more compact spheroids than the $(FFiK)_2$ hydrogel, with spheroid size of around 62 μm (Fig. 7b and f). The interaction between MCF-7 cells and the RGDS sequence displayed on peptide nanofibers might induce the compact spheroid formation. In the case of the $(FFiK)_2$-PHSRN hydrogel, similar spheroid formation was observed (Fig. 7c and f). MCF-7 cells also formed spheroids when cultured in the $(FFiK)_2$-C16 hydrogel (Fig. 7e and f), however, many dead cells were observed after 7 days of cultivation. This result is consistent with the cell proliferation results in the $(FFiK)_2$-C16 hydrogel. C16 stimulates cell receptor *β1* integrin and increases invadopodia activity to promote cell adhesion.[38] This implies that invadopodium activity enhanced the cell adhesion activity but simultaneously induced cell apoptosis.

In contrast, MCF-7 cells proliferated in the $(FFiK)_2$-AG73 hydrogel without significant spheroid formation (Fig. 7d and Fig. S8 m-p). Puchalapalli *et al.* reported the direct binding relationship of AG73 sequences to syndecan in breast cancer cells, which promotes filopodium formation and supports tumor cell adhesion and invasion.[34] Therefore, syndecan and integrin signalling downstream of AG73 might regulate changes in cancer cell behaviour, promoting migration and metastasis activity. The increased number of dead cells observed (Fig. 7d) with a prolonged culture period might be due to the aggregation of conjugated peptides (opaque gel) formed in AG73 and the induction of apoptosis in encapsulated cells. This might cause the slower cell proliferation rate observed in the 3D $(FFiK)_2$-AG73 (Fig. 6b).

3.7. Immunostaining of MCF-7 cells cultured in 3D hydrogels

To investigate the effect of bioactive sequences on the 3D culture of

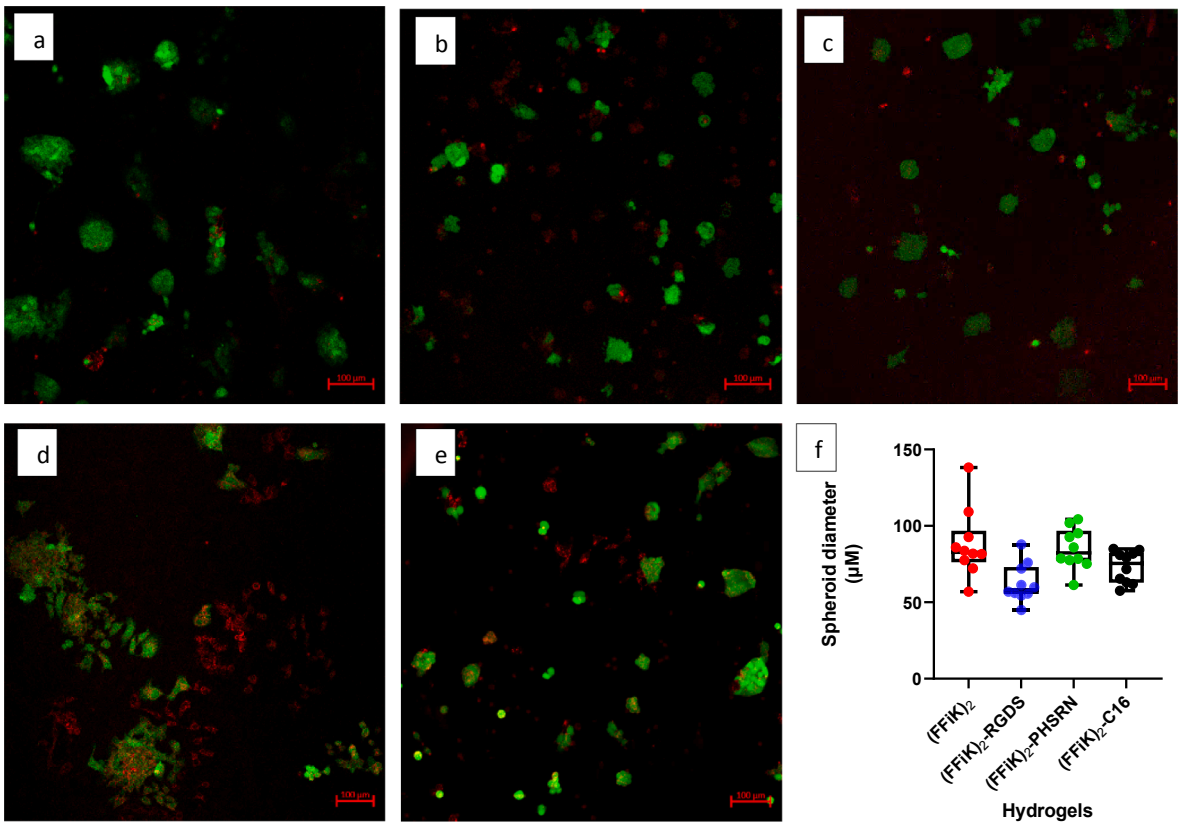

Fig. 7. Confocal imaging of sfGFP-MCF-7 cells at Day 5 in 3D hydrogels. Confocal images of sfGFP-MCF-7 cells embedded within hydrogels on day 5. Dead cells were stained with propidium iodide (PI). (a) $(FFiK)_2$ (b) $(FFiK)_2$-RGDS (c) $(FFiK)_2$-PHSRN (d) $(FFiK)_2$-AG73 (e) $(FFiK)_2$-C16. (f) The diameter of 3D spheroids formed in $(FFiK)_2$, $(FFiK)_2$-RGDS, $(FFiK)_2$-PHSRN and $(FFiK)_2$-C16 hydrogels. Scale bar is 100 μm.

MCF-7 cells, we focused on E-cadherin, a cell adherent protein, because MCF-7 cells cultured in the $(FFiK)_2$ hydrogel formed spheroids, but MCF-7 cells cultured in the $(FFiK)_2$-AG73 hydrogel did not form spheroids. E-cadherin and actin filaments were visualized by immunostaining after 10 days of cultivation in each hydrogel (Fig. 8). In the case of the $(FFiK)_2$ hydrogel, E-cadherin localized on the cell membrane of MCF-7 cells and formed tight adhesion between cells (Fig. 8a). E-cadherin is a mediator of cell-cell adhesion,[39] and actin filaments mediate cell shape, spreading and migration.[40,41] F-actin stained with phalloidin-iFluoro633 co-localized well with E-cadherin. These results correspond to a previous report on spheroid formation by cancer cells.[42] In cases of the $(FFiK)_2$-RGDS and $(FFiK)_2$-PHSRN hydrogels, the expression and localization of E-cadherin and F-actin were similar to the case of the $(FFiK)_2$ hydrogel (Fig. 8b, c). There was no significant difference in the expression level of E-cadherin among the $(FFiK)_2$, $(FFiK)_2$-RGDS and $(FFiK)_2$-PHSRN hydrogels (Fig. S9). These results indicate that the short sequences RGDS and PHSRN do not have a significant effect on the spheroid formation of MCF-7 cells in 3D hydrogels. In the case of the $(FFiK)_2$-C16 hydrogel, although E-cadherin localized on the cell membrane, including cell-cell interfaces, F-actin was not observed at cell-cell interfaces (Fig. 8e). In addition, filopodium-like structures were observed on MCF-7 cells (Fig. S10b). Since C16 promotes cancer cell migration,[38] actin filaments might not be observed at cell-cell interfaces.

In contrast, E-cadherin did not localize to the cell membrane in MCF-7 cells cultured in the $(FFiK)_2$-AG73 hydrogel (Fig. 8d). In addition, tight adhesion between cells was not formed, and F-actin was not observed in many cells. The expression level of E-cadherin in the $(FFiK)_2$-AG73 hydrogel decreased compared to that in the $(FFiK)_2$ hydrogel. These results indicate that the AG73 sequence disrupts cell-cell interaction by down regulating E-cadherin and F-actin proteins. The AG73 sequence binds to syndecan receptors on breast cancer cells and increases the filopodium formation.[34] Filopodium-like structures were also observed on MCF-7 cells (Fig. S10a), therefore, AG73 could affect cell adhesion and invasion through filopodia in the tumor environment and subsequently disrupt the cell assembly.

4. Conclusion

We successfully functionalized the self-assembling peptide $(FFiK)_2$ with bioactive sequences derived from fibronectin and laminin to confer biological functions on $(FFiK)_2$-based hydrogels. Not only short sequences (RGDS and PHSRN) but also long sequences (AG73: RKRLQVQLSIRT and C16: KAFDITYVRLKF) could be conjugated with $(FFiK)_2$ on the solid support. FTIR spectral study revealed that all $(FFiK)_2$ derivatives could assemble into β-sheet structures. TEM observations revealed that $(FFiK)_2$-RGDS could self-assemble into uniform nanofibers. Although other $(FFiK)_2$ derivatives could not form nanofibers alone, co-assembly with the parent $(FFiK)_2$ allowed them to form nanofibrous structures and hydrogels displaying bioactive sequences. In cell experiments, functionalized hydrogels showed superior adhesion of MCF-7 cells to the $(FFiK)_2$ hydrogel. MCF-7 cells were successfully encapsulated in all hydrogels and cultured over 7 days without significant cytotoxicity. In addition, all hydrogel scaffolds were stable under the cell culture conditions over 7 days. During cell proliferation, MCF-7 cells formed spheroids in the $(FFiK)_2$, $(FFiK)_2$-RGDS and $(FFiK)_2$-PHSRN hydrogels. Spheroid formation was also observed in the $(FFiK)_2$-C16. In contrast, MCF-7 cells did not form spheroids and migrate in the $(FFiK)_2$-AG73 hydrogel. Immunostaining experiments revealed that cell-cell interaction was disrupted by AG73, causing cell migration in the hydrogel. Based on these results, we could identify the proper bioactive sequences RGDS and PHSRN to control spheroid formation and AG73 to induce metastatic activity of MCF-7 cells in 3D hydrogels. Recently, it

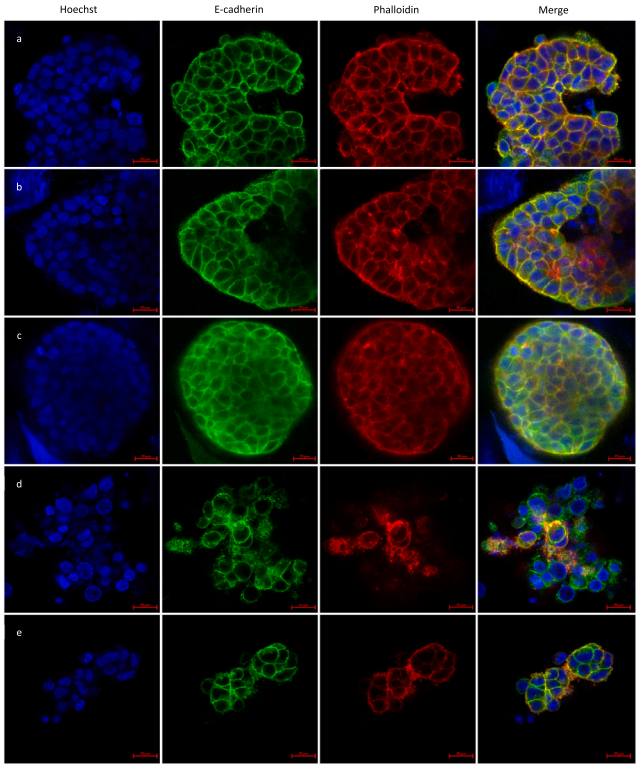

Fig. 8. Immunofluorescent staining of MCF-7 cells cultured within 3D hydrogels. The comparison of MCF-7 cells grown within 3D-$(FFiK)_2$ and derivative hydrogels after 10 days. The nucleus were stained with DAPI (Blue) and cells were counterstained with E-cadherin (Green) and Phalloidin for F-actin (Red). Scale bar is 20 μm. (a) $(FFiK)_2$ (b) $(FFiK)_2$-RGDS (c) $(FFiK)_2$-PHSRN (d) $(FFiK)_2$-AG73 (e) $(FFiK)_2$-C16.

has been reported that tumor-derived spheroids importantly relate to cancer cell stemness with chemoresistance, and high throughput drug screening targeting cancer stem cells is necessary.[43,44] Since the hydrogels functionalized with RGDS and PHSRN sequences induced compact spheroid formation of breast cancer cells, our hydrogels will be able to apply as a drug screening platform. On the other hand, cancer cell metastasis is one of critical issues for cancer treatment, however, systemic treatments to prevent metastasis of breast cancer cells are still less effective.[45] We demonstrated that the hydrogel functionalized with the AG73 sequence could construct the metastatic model of breast cancer cells, which is helpful not only for the elucidation of breast cancer metastasis but also for drug screening targeting cancer cells under metastatic state. Therefore, functionalization of $(FFiK)_2$-based hydrogels with various bioactive sequences can produce biomaterials useful for the control of cancer cell function, tumor engineering, and drug discovery.

Declaration of Competing Interest

The authors declare that they have no known competing financial interests or personal relationships that could have appeared to influence the work reported in this paper.

Acknowledgements

This work was supported in part by a grant from JSPS KAKENHI (18K05351), MEXT, Japan. We thank the Biomaterials Analysis Division, Tokyo Institute of Technology for the TEM observation and technical support for the confocal microscope observations.

Data availability

The data required to reproduce these findings are available upon request.

Appendix A. Supplementary material

Supplementary data to this article can be found online at https://doi.org/10.1016/j.bmc.2021.116345.

References

1 Ghajar CM, Bissell MJ. Tumor engineering: The other face of tissue engineering. *Tissue Eng - Part A*. 2010;16:2153–2156. https://doi.org/10.1089/ten.tea.2010.0135.
2 Pradhan S, Hassani I, Seeto WJ, Lipke EA. PEG-fibrinogen hydrogels for three-dimensional breast cancer cell culture. *J Biomed Mater Res – Part A*. 2017;105:236–252. https://doi.org/10.1002/jbm.a.35899.
3 Hutmacher DW, Loessner D, Rizzi S, Kaplan DL, Mooney DJ, Clements JA. Can tissue engineering concepts advance tumor biology research? *Trends Biotechnol*. 2010;28:125–133. https://doi.org/10.1016/j.tibtech.2009.12.001.
4 Zhang YS, Duchamp M, Oklu R, Ellisen LW, Langer R, Khademhosseini A. Bioprinting the Cancer Microenvironment. *ACS Biomater Sci Eng*. 2016;2:1710–1721. https://doi.org/10.1021/acsbiomaterials.6b00246.
5 Chai YW, Lee EH, Gubbe JD, Brekke JH, Yamamoto M. 3D Cell culture in a self-Assembled nanofiber environment. *PLoS ONE*. 2016;11:e0162853. https://doi.org/10.1371/journal.pone.0162853.
6 Kirshner J, Chen C-J, Liu P, Huang J, Shively JE. CEACAM1-4S, a cell-cell adhesion molecule, mediates apoptosis and reverts mammary carcinoma cells to a normal morphogenic phenotype in a 3D culture. *Proc Natl Acad Sci USA*. 2003;100:521–526. https://doi.org/10.1073/pnas.232711199.
7 Cavo M, Fato M, Peñuela L, Beltrame F, Raiteri R, Scaglione S. Microenvironment complexity and matrix stiffness regulate breast cancer cell activity in a 3D in vitro model. *Sci Rep*. 2016;6:1–13. https://doi.org/10.1038/srep35367.
8 Reynolds DS, Tevis KM, Blessing WA, Colson YL, Zaman MH, Grinstaff MW. Breast Cancer Spheroids Reveal a Differential Cancer Stem Cell Response to Chemotherapeutic Treatment. *Sci Rep*. 2017;7. https://doi.org/10.1038/s41598-017-10863-4.
9 Fung SY, Yang H, Chen P, Zhang S. Sequence effect of self-assembling peptides on the complexation and in vitro delivery of the hydrophobic anticancer drug ellipticine. *PLoS ONE*. 2008;3:e1956. https://doi.org/10.1371/journal.pone.0001956.
10 Wu H, Zhou T, Tian L, Xia Z, Xu F. Self-Assembling RADA16-I Peptide Hydrogel Scaffold Loaded with Tamoxifen for Breast Reconstruction. *Biomed Res Int*. 2017;2017:1–10. https://doi.org/10.1155/2017/3656193.
11 Panda JJ, Chauhan VS. Short peptide based self-assembled nanostructures: Implications in drug delivery and tissue engineering. *Polym Chem*. 2014;5:4431–4449. https://doi.org/10.1039/C4PY00173G.
12 Tsutsumi H, Mihara H. Soft materials based on designed self-assembling peptides: From design to application. *Mol Biosyst*. 2013;9:609–617. https://doi.org/10.1039/c3mb25442a.
13 Bray LJ, Binner M, Holzheu A, et al. Multi-parametric hydrogels support 3D invitro bioengineered microenvironment models of tumour angiogenesis. *Biomaterials*. 2015;53:609–620. https://doi.org/10.1016/j.biomaterials.2015.02.124.
14 Taubenberger AV, Bray LJ, Haller B, et al. 3D extracellular matrix interactions modulate tumour cell growth, invasion and angiogenesis in engineered tumour microenvironments. *Acta Biomater*. 2016;36:73–85. https://doi.org/10.1016/j.actbio.2016.03.017.
15 Holliday DL, Brouilette KT, Markert A, Gordon LA, Jones JL. Novel multicellular organotypic models of normal and malignant breast: Tools for dissecting the role of the microenvironment in breast cancer progression. *Breast Cancer Res*. 2009;11:1–11. https://doi.org/10.1186/bcr2218.
16 Dhiman HK, Ray AR, Panda AK. Three-dimensional chitosan scaffold-based MCF-7 cell culture for the determination of the cytotoxicity of tamoxifen. *Biomaterials*. 2005;26:979–986. https://doi.org/10.1016/j.biomaterials.2004.04.012.
17 Benton G, Arnaoutova I, George J, Kleinman HK, Koblinski J. Matrigel: From discovery and ECM mimicry to assays and models for cancer research. *Adv Drug Deliv Rev*. 2014;79:3–18. https://doi.org/10.1016/j.addr.2014.06.005.
18 Cavo M, Caria M, Pulsoni I, Beltrame F, Fato M, Scaglione S. A new cell-laden 3D Alginate-Matrigel hydrogel resembles human breast cancer cell malignant morphology, spread and invasion capability observed "in vivo". *Sci Rep*. 2018;8:1–12. https://doi.org/10.1038/s41598-018-23250-4.
19 Huang H, Ding Y, Sun XS, Nguyen TA, Engler AJ. Peptide Hydrogelation and Cell Encapsulation for 3D Culture of MCF-7 Breast Cancer Cells. *PLoS ONE*. 2013;8:e59482. https://doi.org/10.1371/journal.pone.0059482.
20 Sawada T, Tsuchiya M, Takahashi T, Tsutsumi H, Mihara H. Cell-adhesive hydrogels composed of peptide nanofibers responsive to biological ions. *Polym J*. 2012;44:651–657. https://doi.org/10.1038/pj.2012.48.
21 Fukunaga K, Tsutsumi H, Mihara H. Self-assembling peptide nanofibers promoting cell adhesion and differentiation. *Biopolymers*. 2013;100:731–737. https://doi.org/10.1002/bip.22309.

22 Fukunaga K, Tsutsumi H, Mihara H. Self-assembling peptides as building blocks of functional materials for biomedical applications. *Bull Chem Soc Jpn*. 2019;92:391–399. https://doi.org/10.1246/bcsj.20180293.

23 Tsutsumi H, Tanaka K, Chia JY, Mihara H. Short self-assembling peptides with a urea bond: A new type of supramolecular peptide hydrogel materials. *Pept Sci*. 2020:1–13. https://doi.org/10.1002/pep2.24214.

24 Chan WC, White PD. *Fmoc solid phase peptide synthesis*. New York: Oxford University Press; 2000.

25 Lowe SB, Tan VTG, Soeriyadi AH, Davis TP, Gooding JJ. Synthesis and High-Throughput Processing of Polymeric Hydrogels for 3D Cell Culture. *Bioconjug Chem*. 2014;25:1581–1601. https://doi.org/10.1021/bc500310v.

26 Schmidt DR, Kao WJ. Monocyte activation in response to polyethylene glycol hydrogels grafted with RGD and PHSRN separated by interpositional spacers of various lengths. *J Biomed Mater Res A*. 2007;83A:617–625. https://doi.org/10.1002/jbm.a.31270.

27 Fichman G, Gazit E. Self-assembly of short peptides to form hydrogels: Design of building blocks, physical properties and technological applications. *Acta Biomater*. 2014;10:1671–1682. https://doi.org/10.1016/j.actbio.2013.08.013.

28 Kikkawa Y, Hozumi K, Katagiri F, Nomizu M, Kleinman HK, Koblinski JE. Laminin-111-derived peptides and cancer. *Cell Adhes Migr*. 2013;7:150–159. https://doi.org/10.4161/cam.22827.

29 Yamada Y, Katagiri F, Hozumi K, Kikkawa Y, Nomizu M. Cell behavior on protein matrices containing laminin α1 peptide AG73. *Biomaterials*. 2011;32:4327–4335. https://doi.org/10.1016/j.biomaterials.2011.02.052.

30 Surewicz WK, Mantsch HH, Chapman D. Determination of Protein Secondary Structure by Fourier Transform Infrared Spectroscopy: A Critical Assessment. *Biochemistry*. 1993;32:389–394. https://doi.org/10.1021/bi00053a001.

31 Nieberler M, Reuning U, Reichart F, et al. Exploring the role of RGD-recognizing integrins in cancer. *Cancers (Basel)*. 2017;9:116. https://doi.org/10.3390/cancers9090116.

32 Aota S, Nomizu M, Yamada KM. The short amino acid sequence Pro-His-Ser-Arg-Asn in human fibronectin enhances cell-adhesive function. *J Biol Chem*. 1994;269:24756–24761. https://doi.org/10.1016/S0021-9258(17)31456-4.

33 Feng Y, Mrksich M. The synergy peptide PHSRN and the adhesion peptide RGD mediate cell adhesion through a common mechanism. *Biochemistry*. 2004;43:15811–15821. https://doi.org/10.1021/bi049174+.

34 Puchalapalli M, Mu L, Edwards C, et al. The Laminin-α1 Chain-Derived Peptide, AG73, Binds to Syndecans on MDA-231 Breast Cancer Cells and Alters Filopodium Formation. *Anal Cell Pathol (Amst)*. 2019;2019:1–10. https://doi.org/10.1155/2019/9192516.

35 Smuczek B, Santos EdeS, Siqueira AS, Pinheiro JJV, Freitas VM, Jaeger RG. The laminin-derived peptide C16 regulates GPNMB expression and function in breast cancer. *Exp Cell Res*. 2017;358:323–334. https://doi.org/10.1016/j.yexcr.2017.07.005.

36 Nascimento CF, de Siqueira AS, Pinheiro JJV, Freitas VM, Jaeger RG. Laminin-111 derived peptides AG73 and C16 regulate invadopodia activity of a human adenoid cystic carcinoma cell line. *Exp Cell Res*. 2011;317:2562–2572. https://doi.org/10.1016/j.yexcr.2011.08.022.

37 Caires-dos-Santos L, da Silva SV, Smuczek B, et al. Laminin-derived peptide C16 regulates Tks expression and reactive oxygen species generation in human prostate cancer cells. *J Cell Physiol*. 2020;235:587–598. https://doi.org/10.1002/jcp.28997.

38 Siqueira AS, Pinto MP, Cruz MC, et al. Laminin-111 peptide C16 regulates invadopodia activity of malignant cells through β1 integrin, Src and ERK 1/2. *Oncotarget*. 2016;7:47904–47917.

39 Takeichi M. Cadherin cell adhesion receptors as a morphogenetic regulator. *Science (80-)*. 1991;251:1451–1455. https://doi.org/10.1126/science.2006419.

40 Gardel ML, Schneider IC, Aratyn-Schaus Y, Waterman CM. Mechanical integration of actin and adhesion dynamics in cell migration. *Annu Rev Cell Dev Biol*. 2010;26:315–333. https://doi.org/10.1146/annurev.cellbio.011209.122036.

41 Yoshii Y, Waki A, Yoshida K, et al. The use of nanoimprinted scaffolds as 3D culture models to facilitate spontaneous tumor cell migration and well-regulated spheroid formation. *Biomaterials*. 2011;32:6052–6058. https://doi.org/10.1016/j.biomaterials.2011.04.076.

42 Smyrek I, Mathew B, Fischer SC, Lissek SM, Becker S, Stelzer EHK. E-cadherin, actin, microtubules and FAK dominate different spheroid formation phases and important elements of tissue integrity. *Biol Open*. 2019;8. https://doi.org/10.1242/bio.037051.

43 Ishiguro T, Ohata H, Sato Ai, Yamawaki K, Enomoto T, Okamoto K. Tumor-derived spheroids: Relevance to cancer stem cells and clinical applications. *Cancer Sci*. 2017;108:283–289. https://doi.org/10.1111/cas.13155.

44 Yilmazer A. Evaluation of cancer stemness in breast cancer and glioblastoma spheroids in vitro. *3 Biotech*. 2018;8:1–11. https://doi.org/10.1007/s13205-018-1412-y.

45 Redig AJ, McAllister SS. Breast cancer as a systemic disease: A view of metastasis. *J Intern Med*. 2013;274:113–126. https://doi.org/10.1111/joim.12084.